https://doi.org/10.5194/egusphere-2025-1812
Preprint. Discussion started: 30 April 2025

Reconstructing landscapes : an adjoint model of the Stream Power and diffusion erosion equation

Carole Petit[1], Anthony Jourdon[2], and Nicolas Coltice[1]

[1]Université Côte d'Azur, CNRS, Observatoire de la Côte d'Azur, IRD, Géoazur, 250 rue Albert Einstein, Sophia Antipolis, 06560 Valbonne, France
[2]Sorbonne Université, CNRS, Institut des Sciences de la Terre de Paris, ISTeP, F-75005 Paris, France

Correspondence: Carole Petit (carole.petit@univ-cotedazur.fr)

Abstract. We simulate landscape evolution using a diffusion–advection equation, where the advection velocity is derived from the erodibility parameters of the Stream Power Law. This formulation allows for forward modeling within a finite-element framework, and enables the use of adjoint methods for sensitivity analysis and parameter inversion—specifically for spatially variable erodibility and diffusion coefficients. When considered individually, model parameters such as the diffusion coefficient, erodibility, initial topography, and time-dependent uplift can be inverted using constraints from final topography, sediment flux, or cumulative denudation at specific locations. Sensitivity analysis on a real landscape reveals that sensitivity to erosion parameters is higher in steep, high-relief areas and that hillslope diffusion and fluvial incision affect the model differently. We apply the adjoint model to two natural cases: (1) reconstructing the pre-incision topography of the southeastern French Massif Central, which appears as a smooth, flat footwall bounded by a linear escarpment along a major lithological boundary; and (2) estimating the Quaternary uplift rate along the Wasatch Range, USA, where our model suggests a significant increase in uplift from 0.2 to 1 $\mathrm{mm.yr}^{-1}$ over the last $\sim$2 million years, consistent with recent geological estimates.

1 Introduction

Tectonic events coupled to climatic variations shape the Earth's surface. These processes result from thousands to millions of years of evolution. Although modern climate, topography, and fluvial activity can be recorded and monitored, reconstructing past landscape evolution remains challenging. To establish relationships between geological constraints like lithological variations and uplift, and erosion-sedimentation mechanisms that quantify sensitivity to fluvial incision or hillslope processes, Landscape Evolution Models (LEMs) have been developed (e.g., Tucker and Slingerland, 1994; Tucker et al., 2001; Davy and Lague, 2009; Tucker and Hancock, 2010; Braun and Willett, 2013; Carretier et al., 2016; Salles and Hardiman, 2016).

The majority of Landscape Evolution Models (LEMs) are forward models: they rely on assumptions about initial and boundary conditions and are validated retrospectively by comparing their results to available data on surface morphometry, sedimentation, exposure age dating, or low-temperature thermochronology. These models often incorporate a wide range of parameters to describe how interactions between climate, lithology, sediment granulometry, isostasy, and/or tectonics influence landscape evolution (Carretier et al., 2016; Salles, 2016; Braun and Willett, 2013; Tucker et al., 2001). As the number of parameters increases to account for various forcings and physical processes, it can become difficult to isolate the influence of each pa-

https://doi.org/10.5194/egusphere-2025-1812
Preprint. Discussion started: 30 April 2025

rameter on the final result. Moreover, the significance of geomorphological observations in constraining model outputs—i.e., identifying which observations are most informative with respect to the model parameters—is generally unknown. As different sets of parameters can produce similar "final" topographies, another difficulty lies in the non-uniqueness of the model. Additionally, the model implementation itself—including the choice of more or less complex physical laws for erosion, transport, sedimentation, and tectonics—can affect model results and performance. These differences in implementation also complicate sensitivity analysis and model validation (Barnhart et al., 2020b).

The questions that arise from being able to "read" the landscape and understand its past and present behaviour can be addressed by inverse models. Although less prevalent in geomorphology than in other geoscience disciplines, inverse approaches have successfully constrained erosion parameters (Croissant and Braun, 2014), their temporal variations (Chandra et al., 2019), and the paleotopography and uplift history of specific regions (Pedersen et al., 2018). These models can integrate fluvial and hillslope erosion, marine deposition, and lithospheric isostatic response, and are sometimes coupled with thermokinematic models to incorporate low-temperature thermochronology data as additional constraints (Braun, 2003; Braun et al., 2012). However, such approaches often struggle to quantify the relative influence of individual model parameters or the impact of different formulations on the final result. To address this limitation, Barnhart et al. (2020b, c) conducted forward multi-model analyses to gain insights into the role of various model processes and parameters on the final output. All these studies highlight the potential of inverse modeling to improve our understanding of landscape evolution, enhance parameter estimation, and quantify uncertainties. However, most of these inverse modeling approaches rely on comprehensive sampling of the parameter space, which can be computationally expensive and time-consuming.

As LEMs often involve a large number of parameters, such gradient-free methods are not always the best choice, due to their computational cost. In contrast, the adjoint method enables efficient sensitivity analysis and the inversion of unknown parameters by a cost-effective, gradient-based approach. Despite their potential, the use of adjoint models in geomorphology remains limited, with few exceptions in related fields such as turbidity currents modeling (Parkinson et al., 2017), terrain correction for weather forecasting (Tao et al., 2019) or hydrodynamics (Clare et al., 2022). The adjoint method involves solving an additional partial differential equation (PDE), called the adjoint equation, which provides information about how changes in the model's output variables affect the objective function (or cost function) that is being optimized (e.g., Talagrand, 2010; Givoli, 2021). By solving both the forward and adjoint equations simultaneously, the adjoint method enables the calculation of gradients or sensitivities with respect to input parameters.

2 Landscape evolution model

Landscape evolution models in their simplest configuration aim at solving:

$$\frac{\partial h}{\partial t} = \nabla \cdot (\kappa \nabla h) - K_f A^m S^n + U, \tag{1}$$

where h is the elevation [L], S is the local channel slope, and $\frac{dh}{dt}$ is the rate of change of elevation over time [L.T^{-1}]. Eq. (1) combines a diffusion term, represented by $\nabla \cdot (\kappa \nabla h)$ that accounts for hillslope processes and the progressive smoothing of

https://doi.org/10.5194/egusphere-2025-1812
Preprint. Discussion started: 30 April 2025

the landscape (with κ the diffusion coefficient [$\mathrm{L}^2.\mathrm{T}^{-1}$]), and a fluvial erosion term, represented by $K_f A^m S^n$, capturing the incision of bedrock river channels known as the Stream Power Law (SPL) (Whipple and Tucker, 1999). Here, K_f represents the rock erodibility [$\mathrm{L}^{1-2\mathrm{m}}.\mathrm{T}^{-1}$], A corresponds to the drainage area [L^2], and m is an exponent related to the area. The parameter n controls the non-linearity of the fluvial erosion, and U is the uplift rate [$\mathrm{L}.\mathrm{T}^{-1}$], accounting for tectonic and/or isostatic uplift.

Eq. (1) can be modified into a diffusion-advection equation (Simpson and Schlunegger, 2003; Braun and Willett, 2013) considering three modifications:

1. The local channel slope S is replaced by the topographic gradient ∇h, as it should be in a classical advection equation.
2. The exponent n is set to 1 in order to insure a linear dependence of the advection term to the topographic gradient.
3. The term $K_f A^m$ is the norm of a velocity vector $K_f A^m \mathbf{u}$, where $\mathbf{u}$ is a unit vector trending parallel to the drainage direction. This velocity vector can, for instance, represent the rate of knickpoint propagation in the drainage system.

These modifications of Eq. (1) lead to the following equation:

$$\frac{\partial h}{\partial t} - \nabla \cdot (\kappa \nabla h) + \mathbf{c} \cdot \nabla h = U, \tag{2}$$

where U is a time-dependent source e.g., the rocks uplift-rate, κ is the diffusion coefficient, and $\mathbf{c}$ is the advection velocity defined as:

$$\mathbf{c} = K_f A^m \mathbf{u}. \tag{3}$$

For our study, we consider an incompressible flow i.e., $\nabla \cdot \mathbf{c} = 0$ because $\mathbf{c}$ represents the velocity at which information propagates, rather than the movement of physical substances like heat or pollutants and cannot therefore be created or absorbed.

The first modification implies that the direction of the local channel slope is as close as possible to that of the topographic gradient. Hence, too large approximations on the direction of the topographic gradient when computing the river network would therefore be a strong limitation to the use of Eq. (1) as a diffusion-advection equation. In many LEMs, due to the discretization of the topographic grid and the use of single-flow direction water routing algorithms, the computed drainage direction is not always co-linear with the topographic gradient as it should be. Certain routing algorithms, such as the D_∞ method (Tarboton, 1997), distribute water flux between two nodes with links oriented closely to the gradient direction, which permits to minimize the orientation discrepancy between the drainage direction and the true topographic gradient. For this reason, we choose to use this algorithm to compute the drainage area and its evolution.

Using the gradient of the elevation, ∇h, for the advection in Eq. (1) offers several advantages. First, we formulate the problem as a diffusion-advection PDE, enabling the use of well-established numerical methods like the finite element (FE) method to solve it. Secondly, in a diffusion-advection equation, the quantity to be diffused and advected is expected to be the same i.e., in our case the topographic "slope", ∇h. However, while in Eq. (1) the diffusive term uses the actual topographic gradient, the fluvial incision term uses the local channel slope, which, depending on the local problem and mesh resolution

https://doi.org/10.5194/egusphere-2025-1812
Preprint. Discussion started: 30 April 2025

may not correspond to the topographic gradient resulting in a physically meaningless quantity. Thirdly, this approach naturally propagates information upstream by advecting topographic characteristics with a velocity proportional to the drainage area in the direction of the gradient resulting in two important features: (1) along channel sides, altough slow, the advection velocity can be nonzero, allowing channel widening with time and (2) along channel paths, despite small slopes, the advection is more pronounced thanks to the large drainage area. Finally, using a well defined advection-diffusion PDE allows us using well sounded methods to compute the adjoint equation of Eq. (2).

To solve Eq. (2), the system is closed with the initial and boundary conditions:

$$h = h_0 \qquad \forall \mathbf{x} \in \Omega \text{ and } t = 0,$$
$$h = g \qquad \forall \mathbf{x} \in \partial\Omega \text{ and } \forall \mathbf{t} \in [0, T],$$

where Ω is the domain of definition, $\partial\Omega$ its boundaries and T the model duration.

To solve Eq. (2), we employ the finite element discretization using Q_1 elements. Introducing the test function $w \in H_1(\Omega)$ the weak form of this equation writes:

$$\int_\Omega w \frac{\partial h}{\partial t} \mathrm{d}V + \int_\Omega w\mathbf{c} \cdot \nabla h \, \mathrm{d}V + \int_\Omega \nabla w \cdot (\kappa \nabla h) \, \mathrm{d}V - \int_{\partial\Omega} w\mathbf{q} \cdot \mathbf{n} \, \mathrm{d}S = \int_\Omega wU \, \mathrm{d}V \tag{4}$$

where $\mathbf{q} = \kappa \nabla h$ is the sediment flux from the hillslope diffusion, and $\mathbf{n}$ is the unit vector pointing outward normal to the boundary $\partial\Omega$.

In this study, we present a new method to both solve the forward (Eq. 2) and adjoint PDEs describing landscape evolution and we demonstrate its ability to reconstruct the initial conditions, source term and erosion coefficients that are the principal control parameters of LEMs. The method utilizes components of the Landlab toolbox (Hobley et al., 2017; Barnhart et al., 2020a; Hutton et al., 2020) to remove local minima from the initial topography, compute the drainage area and catchment indexing while the FE discretization and numerical solution are done using the Firedrake software (Ham et al., 2023). At a given timestep k, the topography computed at timestep $k-1$ is used to calculate the drainage area and corresponding advection velocity, which are then employed to solve for the updated topography. In addition, the output sediment flux is stored as the total volume of eroded rocks, and can be further used in the adjoint model as a constraint for the inversion.

3 Adjoint method

3.1 Governing equations

We consider the PDE describing the evolution of surface elevation h as in Equation 2. We rewrite this equation in the residual form $Lh - f = 0$, where: $L := L(p)$ is a differential operator acting on h, such as:

$$Lh = \frac{\partial h}{\partial t} + \mathbf{c} \cdot \nabla h - \nabla \cdot (\kappa \nabla h), \tag{5}$$

and f is the source term, which in this case corresponds to the uplift rate U. The solution $h := h(p)$ of this PDE is controlled by a set of parameters p (initial conditions, h_0, , velocity, $\mathbf{c}$, diffusivity, κ, and source term, U).

https://doi.org/10.5194/egusphere-2025-1812
Preprint. Discussion started: 30 April 2025

We define a cost functional $J := J(h)$ that has to be minimized:

$$J = \int_{\Omega} g(h)\mathrm{d}V, \tag{6}$$

where $g(h)$ can be defined as residual between output topography at time T and observations h_{obs} such as:

$$g(h_T) = \frac{1}{2}(h_T - h_{obs})^2 \tag{7}$$

and its derivative with respect to h is:

$$g'(h) = \frac{\partial g}{\partial h} = h - h_{obs} \tag{8}$$

The objective is to evaluate the gradient $\frac{dJ}{dp}$, which will then allows us either to minimize J (for parameter optimization) or to analyze the influence of certain parameters on the model result (for sensitivity analysis). To this end, we first solve the forward problem using a trial parameter value p, and then compute the adjoint variable λ by solving the adjoint equation:

$$L^\dagger \lambda = g', \qquad \forall \lambda \in \Omega, \tag{9}$$

$$\lambda = 0 \qquad \forall \lambda \in \partial\Omega. \tag{10}$$

Here $L^\dagger$ is the formal adjoint of the operator L. For advection-diffusion equations, the adjoint operator has the same form as the forward operator, except that the advection velocity $\mathbf{c}$ is reversed (e.g., Celia et al., 1990):

$$L^\dagger \lambda = \frac{\partial \lambda}{\partial t} - \mathbf{c} \cdot \nabla\lambda - \nabla \cdot (\kappa \nabla \lambda). \tag{11}$$

First, we have to solve for λ in Equation 9, where the forcing term is g'. Once the adjoint variable λ is computed, we use it to evaluate the gradient of the cost functional with respect to the parameter p:

$$\frac{\mathrm{d}J}{\mathrm{d}p} = -\int_{\Omega} h \frac{\partial L^\dagger}{\partial p} \lambda \mathrm{d}V\,. \tag{12}$$

The partial derivative $\frac{\partial L}{\partial p}$ can be computed analytically when possible, or numerically. The functional J may also incude time-dependent controls, in which case it will integrate the misfit between models and observations over the model duration T.

The computational workflow is as follows:

1. Solve the forward problem $Lh - f = 0$ for a given parameter value p,
2. Solve the adjoint problem for λ using Equation (9),
3. Compute the gradient $\frac{\mathrm{d}J}{\mathrm{d}p}$ using Equation (12),
4. Update the parameter p using an optimization algorithm, and iterate until convergence.

https://doi.org/10.5194/egusphere-2025-1812
Preprint. Discussion started: 30 April 2025

In practice, the Firedrake package automates this process using automatic differentiation (AD) techniques. The user only needs to define the weak form of the PDE and specify the functional J.

In our problem, the objective function J combines data misfit terms (comparing modeled and observed topography, sediment flux, or denudation rates) with regularization components. To recover solutions with sharp discontinuities while preserving smooth regions, we employ total variation (TV) regularization (Strong and Chan, 2003). For initial condition inversion (h_{init}), we implement an edge-preserving TV scheme adapted from image processing techniques (Barcelos, 2002):

$$J_{\text{reg}} = \int_\Omega \left[\alpha g \|\nabla h\| + \frac{1}{2}(1-g)(h-h_{\text{obs}})^2 \right] \mathrm{d}V, \tag{13}$$

$$g = \left(1 + k|\nabla G * h|^2\right)^{-1}, \tag{14}$$

where $\alpha > 0$ controls the regularization strength, $g \in (0, 1]$ is an edge-detection function using Gaussian-filtered (G) topography gradients,and k modulates edge sensitivity. We calibrate the parameters α and k to suppress high-frequency noise in reconstructed solutions and preserve geomorphologically significant sharp features (e.g., fault scarps, knickpoints). Beyond parameter inversion, the adjoint directly provides the model relative (dimensionless) sensitivity to a parameter p through:

$$S_p^{\text{rel}} = \frac{p}{J}\frac{\partial J}{\partial p}, \tag{15}$$

where all physical quantities are non-dimensionalized to ensure consistent scaling of residuals and sensitivities. This formulation provides dimensionless sensitivity measures enabling cross-parameter comparison.

3.2 Cost functional

Before we consider the natural cases of the French Massif Central and Wasatch Range presented in section 4.2.4, we first conduct synthetic experiments by running first the forward FE model to generate synthetic data (e.g., topography, sediment flux, and/or cumulative denudation over time). We then use these data as controls for sensibility analysis and/or inversion of the main model parameters: initial conditions, erodibility, diffusion coefficient, and source term. In the adjoint method, the forward model is executed once, starting with an initial guess that is slightly different from the value used for generating the synthetic data. In certain inversion procedures, we re-run the forward model using the inverted parameters to compare model outputs (topography, sediment flux, etc.) with synthetic data. Initial topographic conditions for the forward model can consist of simple geometric shapes (linear drainage divide, linear escarpment) or can be derived from an existing digital elevation model (DEM). For instance, for testing the model capacity to reconstruct spatial variations of κ and K_f, we use as initial conditions the same DEM as in section 4.2.4 i.e., the south-east border of the French Massif Central, which permits to evidence spatially variable model sensitivity to erosion parameters. For all cases, we define the functional J as follows:

$$J = \frac{1}{2}\int_\Omega (h-h_{obs})^2\,dV + C\sum_{i=0}^{t_{max}}(q_i - q_{i_{obs}})^2\Delta t + D\sum_{j=0}^{N}\sum_{i=0}^{t_{max}}(d_{ij} - d_{ij_{obs}})^2\Delta t + \text{regularization terms} \tag{16}$$

https://doi.org/10.5194/egusphere-2025-1812
Preprint. Discussion started: 30 April 2025

The first term of the functional represents the misfit between the modelled topography, h, and the observed topography, h_{obs}, integrated over the entire domain Ω. The second term incorporates a penalization of the differences between the estimated outgoing sediment flux, q, and the true sediment flux, q_{obs}, summed over discrete time intervals corresponding to the model timestep Δt. The third term represents the difference between observed and modelled cumulated denudation, d, with time on some prescribed nodes n that could correspond to sampling points. Finally, the coefficients C and D control the relative importance of the sediment flux and denudation residual terms in the inversion. Depending on the parameter we want to analyse, coefficients C and/or D may be zero.

4 Results

4.1 Taylor test of the adjoint model

We first test the consistency of the adjoint model using a Taylor test on an initial forward model consisting of a $40\ \mathrm{km} \times 40\ \mathrm{km}$ domain, with a $20\ \mathrm{km} \times 20\ \mathrm{km}$ square mountain at the center uplifting at a constant rate of $0.5\ \mathrm{mm.yr}^{-1}$. The Taylor test verifies that:

$$J(m + \epsilon \partial m) - J(m) - \epsilon \nabla J \cdot \partial m \to 0 \quad \text{at} \quad \mathcal{O}(\epsilon^2), \tag{17}$$

where m is the control parameter of interest, ∂m is a small perturbation of this parameter, and ϵ is a small value. The Taylor test consists of applying a perturbation to the initial erodibility coefficient K_f, computing the second-order Taylor remainder using Eq. (17), then successively decreasing ϵ and verifying that the residual decreases at the expected order of ϵ^2.

The results of the Taylor test applied to this model show that the residuals are consistent with theoretical predictions (Fig. 1), exhibiting a convergence rate close to 2 down to ϵ values of $\sim 5 \times 10^{-11}$. Beyond this threshold, the convergence deteriorates, and the residual fluctuates between 10^{-10} and 10^{-8}. Although this threshold is much larger than machine precision ($\sim 2 \times 10^{-16}$), this result indicates that the adjoint model is robust even for very small perturbations (Fig. 1).

4.2 Sensitivity analysis and inversion

4.2.1 Erosion parameters

We evaluate the model sensitivity and its capability to reconstruct spatially variable erosion coefficients K_f and κ on a $190\ \mathrm{km} \times 190\ \mathrm{km}$ grid with 128×128 elements. The initial topography is similar to the target topography used in Section 4.2.4 for initial condition inversion — specifically, a dissected NE-SW linear escarpment marking the southeastern boundary of the French Massif Central (Fig. 2a, 3, and 4).

In the first test, we assume spatially uniform values of $K_f = 5 \times 10^{-7}\ \mathrm{yr}^{-1}$ and $\kappa = 3 \times 10^{-2}\ \mathrm{m}^2.\mathrm{yr}^{-1}$, and independently compute the relative model sensitivity S_p^{rel} to each parameter. The sensitivity values for κ are generally low, except in two distinct regions: the NW corner of the domain, where the Cenozoic Cantal stratovolcano is located, and a NE-SW elongated zone corresponding to the southeastern escarpment of the Massif Central (Fig. 2b). The model sensitivity to the K_f coefficient

https://doi.org/10.5194/egusphere-2025-1812
Preprint. Discussion started: 30 April 2025

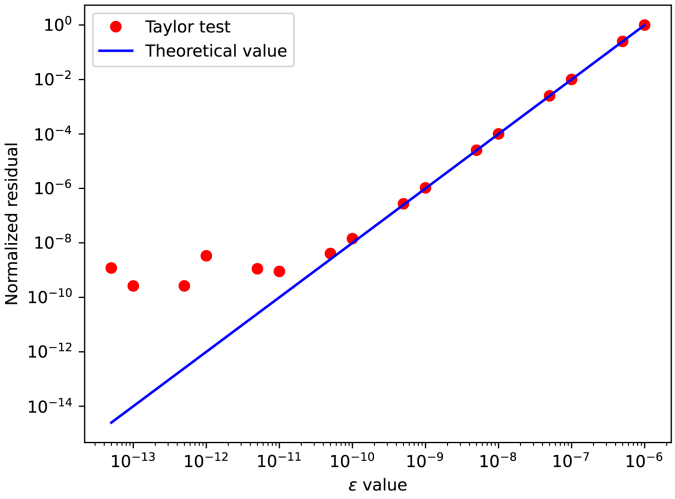

Figure 1. Taylor test on the erodibility coefficient K_f using an initial ϵ value of 1×10^{-6} (upper right point).

Model n°	IC	Dimensions, Resolution m^2, elem	Type	Duration	κ $m^2.yr^{-1}$	K_f yr^{-1}	$U(t)$ $mm.yr^{-1}$	Figure n°
1	Square	$(4 \times 10^4)^2$, 128×128	Taylor test	0.5 Ma	10^{-2}	3×10^{-6}	0.5	1
2	Square	$(19 \times 10^4)^2$, 128×128	Analysis	1 Ma	*variable*	5×10^{-7}	0	2b
2	Square	$(19 \times 10^4)^2$, 128×128	Analysis	1 Ma	10^{-3}	*variable*	0	2c
3	Square	$(19 \times 10^4)^2$, 128×128	Inversion	1 Ma	X	5×10^{-7}	0	3
4	Square	$(19 \times 10^4)^2$, 128×128	Inversion	1 Ma	10^{-3}	X	0	4
5	X (**Scarp**)	$(4 \times 10^4)^2$, 128×128	Inversion	1 Ma	5×10^{-3}	3×10^{-6}	0	5
6	Square	$(4 \times 10^4)^2$, 128×128	Inversion	4 Ma	5×10^{-3}	4×10^{-6}	X (**0.5**)	6
7	X	$(1.9 \times 10^5)^2$, 128×128	Inversion	4 Ma	10^{-3}	10^{-6}	0	7
8	Divide	$2.2 \times 10^4 \times 1.4 \times 10^4$, 128×80	Inversion	4 Ma	10^{-1}	3×10^{-6}	X	8

Table 1. Summary of models and parameters. IC denotes initial conditions; resolution is the number of elements in the x and y dimensions. For inverse models, the letter X indicates which parameters has been inverted. Numbers in bold within parentheses indicate which actual parameters were used in the corresponding forward model.

200 is somehow larger, especially in the Massif Central region, and is even most pronounced around the headwaters of the major catchments, where topographic slopes are steep (Fig. 2c). Overall, both tests suggest that the model's sensitivity to erosion coefficients is particularly large along the NE-SW trending southern Massif Central escarpment, and very small in the low altitude areas of the Rhône plain.

https://doi.org/10.5194/egusphere-2025-1812
Preprint. Discussion started: 30 April 2025

We then define arbitrarily two simple polygons where these coefficients are different from the background value and then re-run the forward models for 1 Ma. The source term is null, meaning that no uplift is imposed to the surface topography. In the inversion tests, we fix the model duration, initial conditions, source term and either the erodibility or the diffusion coefficient as identical to that of the forward models. With these known values as a starting point, we perform separate inversions to estimate the unknown parameter, either K_f or κ. The primary objective is to evaluate the model capability to accurately retrieve the expected values for these unknown parameters (see Table 1).

We carry out the inversion of the diffusion coefficient κ using only the final topography as the reference "observable" (h_{obs}) to control the inversion. Since hillslope diffusion is a local process, it would not be interesting to use other data representing long-distance sediment transport, such as the outgoing sediment flux, as a control. The "true" κ used in the forward model consists of a backgroud value of 10^{-2} $\mathrm{m}^2.\mathrm{yr}^{-1}$ with two polygons of lower (5×10^{-3} $\mathrm{m}^2.\mathrm{yr}^{-1}$) and higher ($2\times10^{-2}$ $\mathrm{m}^2.\mathrm{yr}^{-1}$) values (Fig. 3a). At the beginning of the inversion procedure, we fix the initial value everywhere as identical to the background value. The inversion of the diffusion coefficient κ converges after 33 iterations and the resulting κ map (Fig. 3b) shows that the inversion correctly retrieves the spatial variations of the κ coefficient, with some lateral smearing.

The inversion of the erodibility coefficient K_f is performed using both the final topography and the time-distributed outgoing sediment flux as observables. The forward model involves a background K_f value of 1×10^{-6} yr^{-1} with two polygons of larger values (2×10^{-6} and 3×10^{-6} yr^{-1}, Fig. 4a). Similarly to the previous case, the initial "guess" value for K_f is identical to the background value. The inversion converges after 31 iterations and the K_f map shows that the areas of different coefficients are very well delineated, although the absolute value reconstructed by the inversion is slightly different and more variable than the actual one (Fig. 4b). In some areas, the model does not depart from the trial value, meaning that the inversion result is not well constrained. In the area of intermediate K_f value initially fixed at 2×10^{-6} yr^{-1}, the mean average value reconstructed by the inversion is too large, while it is correct in the area of initially large K_f value. Nevertheless, the areas with initially different K_f coefficient are precisely reconstructed.

4.2.2 Initial conditions

In this section, we demonstrate the model ability to recover initial conditions when erosion parameters (K_f, κ, m), uplift rate and erosion duration are known. The process begins with a test simulation, lasting for 1 million years, on an initial topography featuring a linear escarpment associated with a random topographic noise with an amplitude of maximum 40 meters, and no uplift (Fig. 5a). The final topography resulting from this simulation shows a strongly incised escarpment, though the surface trace of the fault is still relatively easy to follow. It is then used as the reference observable for the adjoint model, together with the evolution of the outgoing sediment flux with time.

The inversion process starts with an initial guess for the initial conditions, which consists of a linear topographic slope in the same direction as in the forward model, but devoid of any escarpment (Fig. 5b). Starting from this initial guess, the inversion finally retrieves an initial topography close to the actual one (although slightly smoother, Fig. 5c). The inverted initial topography deviates from the initial guess and consists of two flat-lying surfaces separated by a steep escarpment, which is located close to the actual one. The result is obtained after 57 iterations with a coefficient $\alpha = 2\times10^{-4}$ and an edge preservation

https://doi.org/10.5194/egusphere-2025-1812
Preprint. Discussion started: 30 April 2025

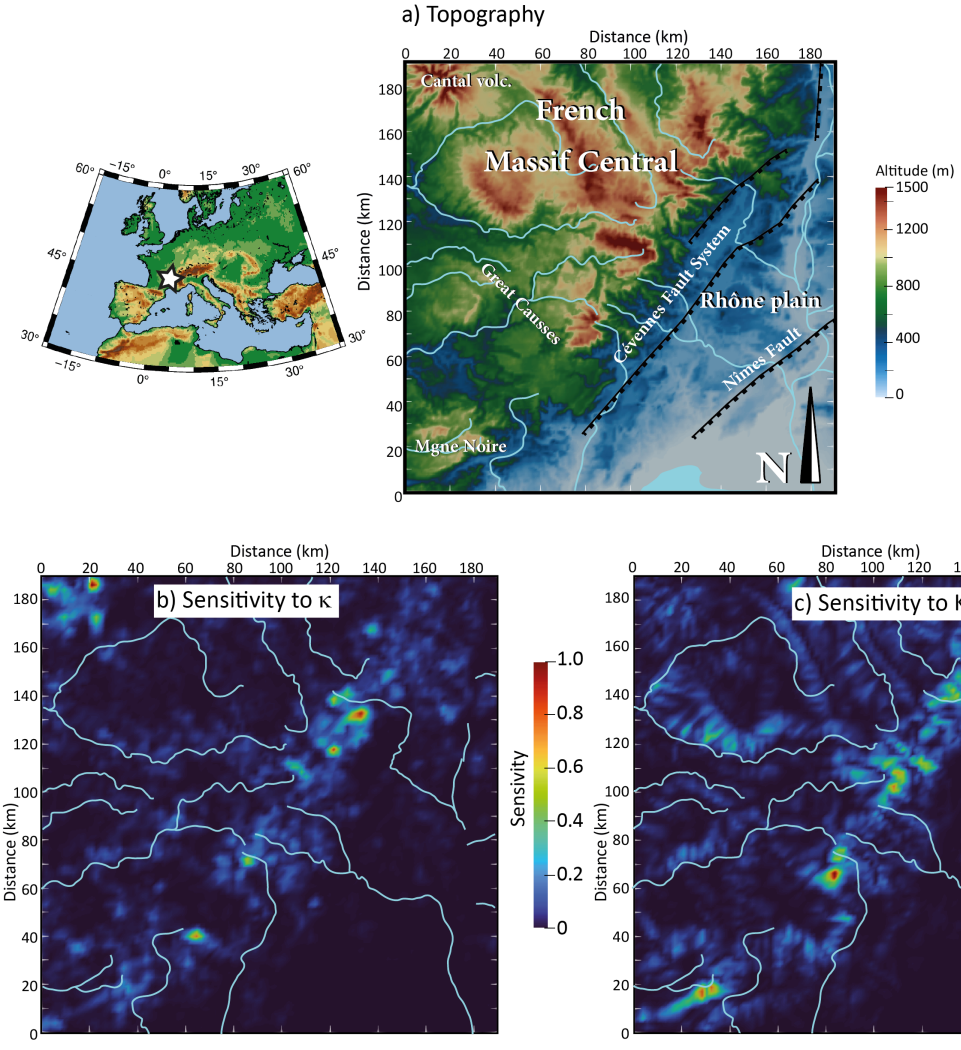

Figure 2. Sensitivity tests on a real topography for the diffusion coefficient $\kappa$and the erodibility coefficient K_f. (a): Topography of the SE part of the French Massif Central with the main drainage systems. White star on the left map indicates the location of the study area. (b): Relative model sensitivity to κ. (c): Relative model sensitivity to K_f.

https://doi.org/10.5194/egusphere-2025-1812
Preprint. Discussion started: 30 April 2025

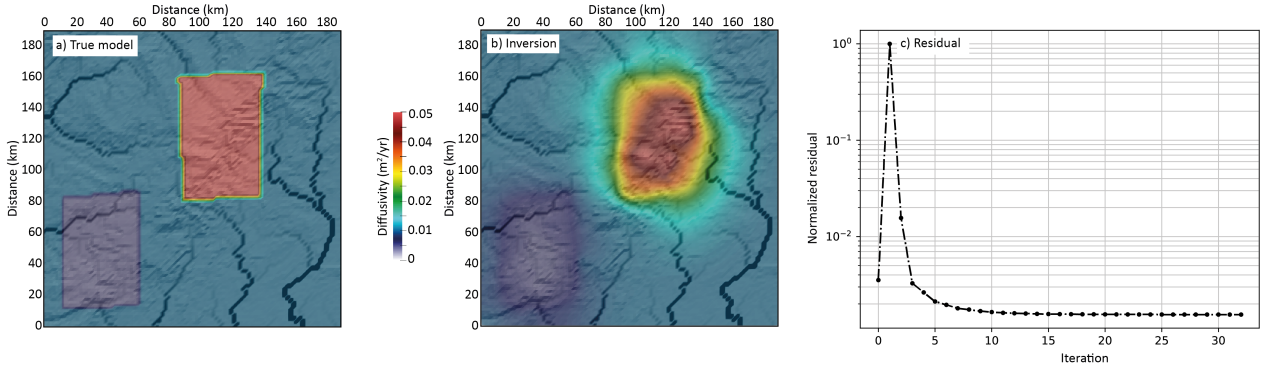

Figure 3. Inversion of the diffusion coefficient κ with the adjoint method. (a): True spatial variations of κ used to build the forward model. (b): inverted κ values map. (c): Inverse model convergence. Same topography as on Figure 2.

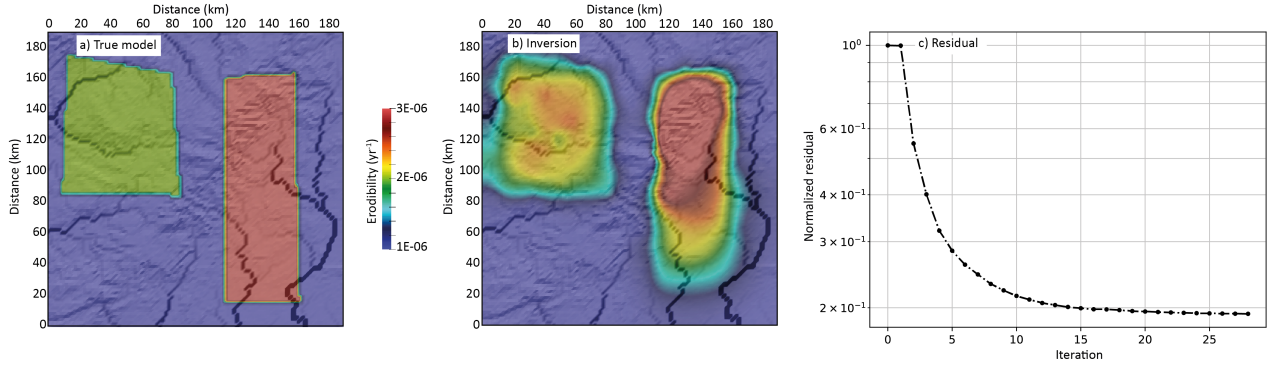

Figure 4. Inversion of the erodibility coefficient K_f with the adjoint method. (a): True spatial variations of K_f used to build the forward model. (b): inverted K_f values map. (c): Inverse model convergence. Same topography as on Figure 2.

coefficient $k = 100$ in Eq. (13). The normalized residual stabilizes around 3×10^{-7} and the modelled sediment flux is very close to the actual one, except in the first steps of the model evolution (Fig. 5d and e).

4.2.3 Source term

We now aim to assess the adjoint method's ability to accurately estimate source term variations, assuming that the boundaries of the uplifting area are known. The forward model simulates a square mountain, similar to Model 1. In this scenario, the mountain experiences a constant uplift rate of 0.5 $\mathrm{mm.yr}^{-1}$ over 4 million years.

In the inversion process, we use the final topography, outgoing sediment flux and cumulative denudation on 3 specific model points as control points on the inversion (Fig. 6a). We run the forward model for a duration of 4 Myrs using a time step of 2,000 years. The topography modelled with the inverted uplift rate value after 4 Ma is very similar to the forward model 1 (Fig. 16a

https://doi.org/10.5194/egusphere-2025-1812
Preprint. Discussion started: 30 April 2025

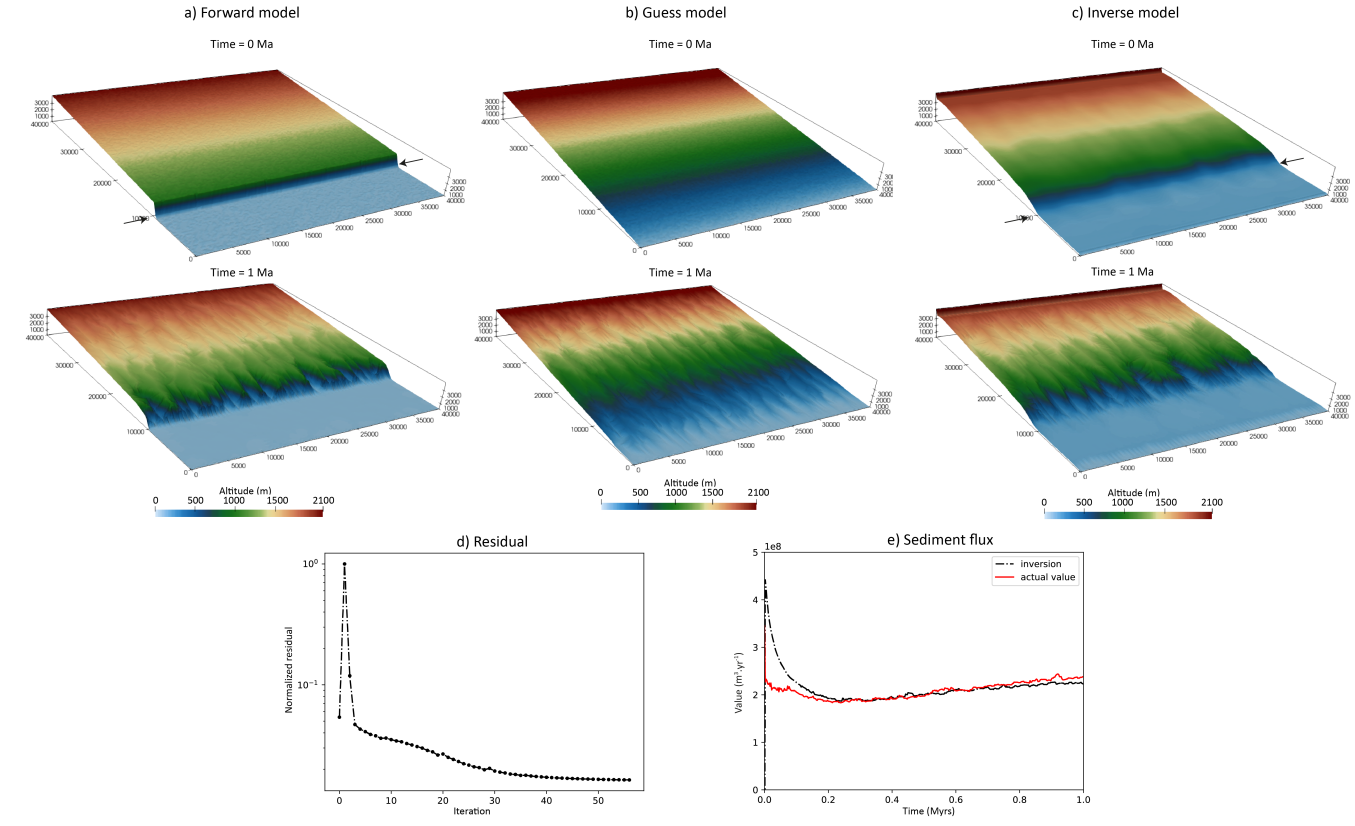

Figure 5. Inversion of initial conditions on a south-facing escapment (model 5, Table 1). Top and middle panels: initial and final (1 Ma) topographies in the forward model, the initial guess and the inversion result (a, b and c, respectively). Bottom panels: Relative residual (d) and modelled sediment flux (e).

and b). The inversion results indicate that the uplift rate value is correctly estimated, with a value ranging from 0.48 $\mathrm{mm.yr^{-1}}$ to 0.51 $\mathrm{mm.yr^{-1}}$ at the end (i.e., with an error of 4 %), with a significant deviation from the initial guess value of 0.2 $\mathrm{mm.yr^{-1}}$ (Fig. 16d). The total outgoing sediment flux and point denudation with time are correctly reproduced (Fig. 16e and f).

4.2.4 Natural cases

In the both following cases, we extract the target topography from the Shuttle Radar Topography Mission database (NASA, 2013) and re-sample it at the desired model resolution.

- *SE Border of the French Massif Central*

Based on the previous results on synthetic data, we now use this approach to reconstruct the topography of the southeastern border of the French Massif Central prior to its latest stage of strong incision by tributaries of the Rhône River drainage

https://doi.org/10.5194/egusphere-2025-1812
Preprint. Discussion started: 30 April 2025

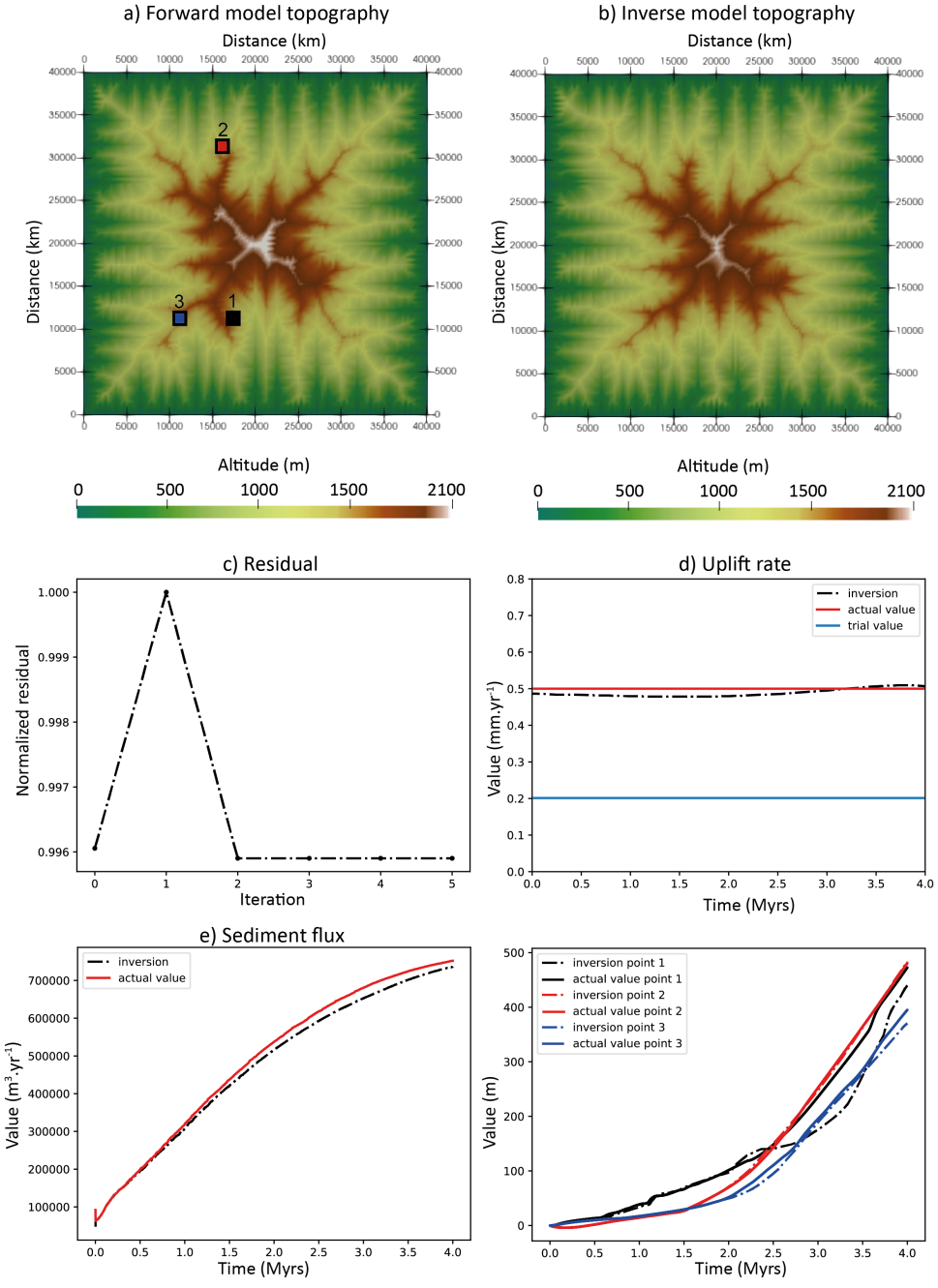

Figure 6. Results of source term (constant uplift rate) inversion (model 6, Table 1). Top: final topography with the actual (a) and inverted (b) uplift rates after 4 Myrs. Middle: normalized functional value (c) and uplift rate (d). Blue line on panel d indicates the trial uplift rate value used in the inversion procedure. (e): outgoing sediment flux from the forward ("actual value") and inverse model ("inversion"). (f): actual and modelled cumulative denudation on the 3 control points (see (a) for point location).

https://doi.org/10.5194/egusphere-2025-1812
Preprint. Discussion started: 30 April 2025

system. The SE border of the Massif Central is a former southeast-facing normal fault escarpment (the Cévennes Fault system) originated mainly from Mesozoic to Cenozoic extensional tectonics (Séranne et al., 2021). The uplift of the Massif Central occurred in several steps since the Paleogene, the last stage being a Late Miocene to Pliocene uplift which resulted into intense fluvial incision observed along its SE border (Olivetti et al., 2016; Fauquette et al., 2020). We cannot accurately constrain time variations of the erosion parameters, which trade off with model duration (the largest the erodibility coefficient, the shortest the time needed to achieve a given amount of erosion). We do not aim, as well, at reproducting peculiar morpho-tectonic events like the Messinian Salinity Crisis, which occurred at the end of the Miocene, and we neglect the — presumably small — topographic uplift that could result from flexural isostatic response to ongoing erosion. Consequently, the initial topography that we will obtain from the adjoint method likely resembles the pre-incision landscape, but its precise age remains unconstrained.

The initial guess for the topography is either (1) a NE-SW trending divide, featuring a gently NW-dipping plane opposite to a steeper SE-dipping surface, or (2) the current topography. In the first case, the maximum altitude is 2000 m, located along the drainage divide, while in the second case, it reaches only 1500 m in the NW corner of the model, which corresponds to the Miocene Cantal stratovolcano. The model runs for 3 Myrs with a diffusion coefficient of 10^{-2} $\mathrm{m}^2.\mathrm{yr}^{-1}$ and an erodibility coefficient of 10^{-6} yr^{-1}. In this inversion, only the final topography serves as a reference observable to compute the functional J. For both initial guesses (divide or current topography), the inverted initial topography reveals a relatively smooth, poorly dissected region in the NW half of the model, representing the footwall of the normal fault system, and a lower-altitude plain in the SE half. In both cases as well, these surfaces are delineated by a linear, well-marked escarpment.

When the initial guess features a smooth topography with a linear drainage divide, the fault escarpment closely follows the observed surface fault traces, particularly in the NW corner of the map, and the average footwall elevation is higher than in the second case. In contrast, the model initialized with the current topography results in lower altitude contrasts and a slightly more sinuous fault escarpment, which is positioned further inland relative to the fault trace. This suggests that using the current topography as an initial guess is less effective in annealing escarpment retreat caused by fluvial incision and predicts a slightly lower average topography compared to the model with a simple linear NE-SW divide.

Geologically, the reconstructed initial conditions from the "divide" model reveal a contrasting landscape within the Cévennes fault system footwall. In the SW, the topography is characterized by a low-altitude (800 m) domain corresponding to the Mesozoic Great Causses and the Variscan Montagne Noire metamorphic massif. To the north lies a moderately elevated region (1000-1400 m), encompassing the crystalline core of the Massif Central. This area features outcropping Variscan metamorphic rocks and granitoids locally overlain by Cenozoic volcanism. At the northeastern edge of the domain, a large circular massif corresponding to the cenozoic Cantal stratovolcano reaches altitudes exceeding 1400 m, however significantly lower than the 2500 m estimated from pollen assemblages prior to its Plio-Pleistocene erosion (Fauquette et al., 2020). In this model, the incision along the southeastern border of the Massif Central by steep, southeastward-flowing streams is largely erased, with only a few notches remaining downstream. In fact, the morphological fault escarment is not aligned with the main Cévennes fault, but runs along the boundary between the crystalline Massif Central and the sedimentary cover of the Rhône plain. This boundary is also marked by a major early Mesozoic normal fault. This suggests that prior to incision, the morphological fault escarpment did not coincide with the main trace of the Cévennes fault, but rather with the mixed tectonic and lithological

https://doi.org/10.5194/egusphere-2025-1812
Preprint. Discussion started: 30 April 2025

contact lying between the Massif Central metamorphic and granitic rocks and the Rhône plain Meso-Cenozoic deposits. On map, the main trace of the Cévennes fault system outcrops within marly Cretaceous deposits, and may never have constituted a major fault scarp.

- *Uplift rate of the Wasatch Fault, Utah*

The Wasatch Fault, in the NE part of the Basin and Range is a well-known active normal fault, having been the focus of numerous tectonic and geomorphological studies since the 1990s. The long-term rock uplift rate of the Wasatch Range in the footwall ranges between 0.6 to 1.2 $\mathrm{mm.yr^{-1}}$ depending on the considered time scale (Ehlers et al., 2003; Friedrich et al., 2003; Stock et al., 2009; Smith et al., 2024). Although footwall uplift began in Miocene times (e.g., Armstrong et al., 2003; Ehlers et al., 2003), it is unlikely that the present landscape preserves traces of the earliest uplift events, as geomorphic processes, particularly regressive erosion, tend to erase older features over time. In this model, we treat the source term (uplift rate) as an unknown parameter and we only use the final topography to compute the functional J. The target topography corresponds to a 14 km-long section of the NS-trending Weber segment of the Wasatch Fault, which separates the Wasatch Range to the east from the Great Salt Lake basin to the west (Fig. 8a). The initial topography reflects the general shape of the Wasatch Range in this area, featuring a NNW-SSE trending ridge with an elevation of 2500 m that overlooks a plain at an elevation of 1300 m (Fig. 8b). The model simulates 4 million years of landscape evolution (Fig. 8c), capturing the time frame during which river incision may still preserve a record of recent uplift history (Smith et al., 2024). We set the erosion parameters as follows: the diffusion coefficient κ is 0.1 $\mathrm{m^2.yr^{-1}}$, and the erodibility coefficient K_f is 3.2×10^{-6} $\mathrm{yr^{-1}}$, close to the values used in previous inverse modeling studies by Smith et al. (2024). The initial guess for the uplift rate is 0.5 $\mathrm{mm.yr^{-1}}$. The residual drops significantly within the first 10 iterations, and the model stops after 24 iterations (Fig. 8d). The estimated uplift rate shows an initial phase with relatively low values (less than 0.2 $\mathrm{mm.yr^{-1}}$), gradually increasing to approximately 1 $\mathrm{mm.yr^{-1}}$ over 4 million years of evolution. This result aligns with the average Quaternary uplift rates obtained from river longitudinal profile inversion (Smith et al., 2024) (Fig. 8e) especially between 2 and 3.2 Ma of model evolution where the mean uplift rate seems to increase regularly. In the last 1 Ma, river profiles tend to indicate a drop in uplift rate values from 0.8 to 0.5 $\mathrm{mm.yr^{-1}}$ while our inversion still predicts an increase. By dividing the modeled outgoing sediment flux by the area of the uplifted region, we estimate average denudation rates ranging from 0.2 to 0.35 $\mathrm{mm.yr^{-1}}$ (Fig. 8f), consistent with values derived from cosmogenic ^{10}Be measurements (Stock et al., 2009).

5 Discussion

These examples highlight the potential of solving a diffusion-advection equation for both forward and adjoint problems in landscape evolution. Notably, the ability to compute model sensitivity to key parameters such as erosion rates, source terms, or initial conditions provides important insights into the dominant drivers of landscape evolution in both generic and case-specific scenarios. Furthermore, this approach widens the scope of data-driven inverse modeling by enabling the integration of diverse constraints, including time-dependent (e.g., denudation rates, sediment flux) and time-independent (e.g., final topography)

https://doi.org/10.5194/egusphere-2025-1812
Preprint. Discussion started: 30 April 2025

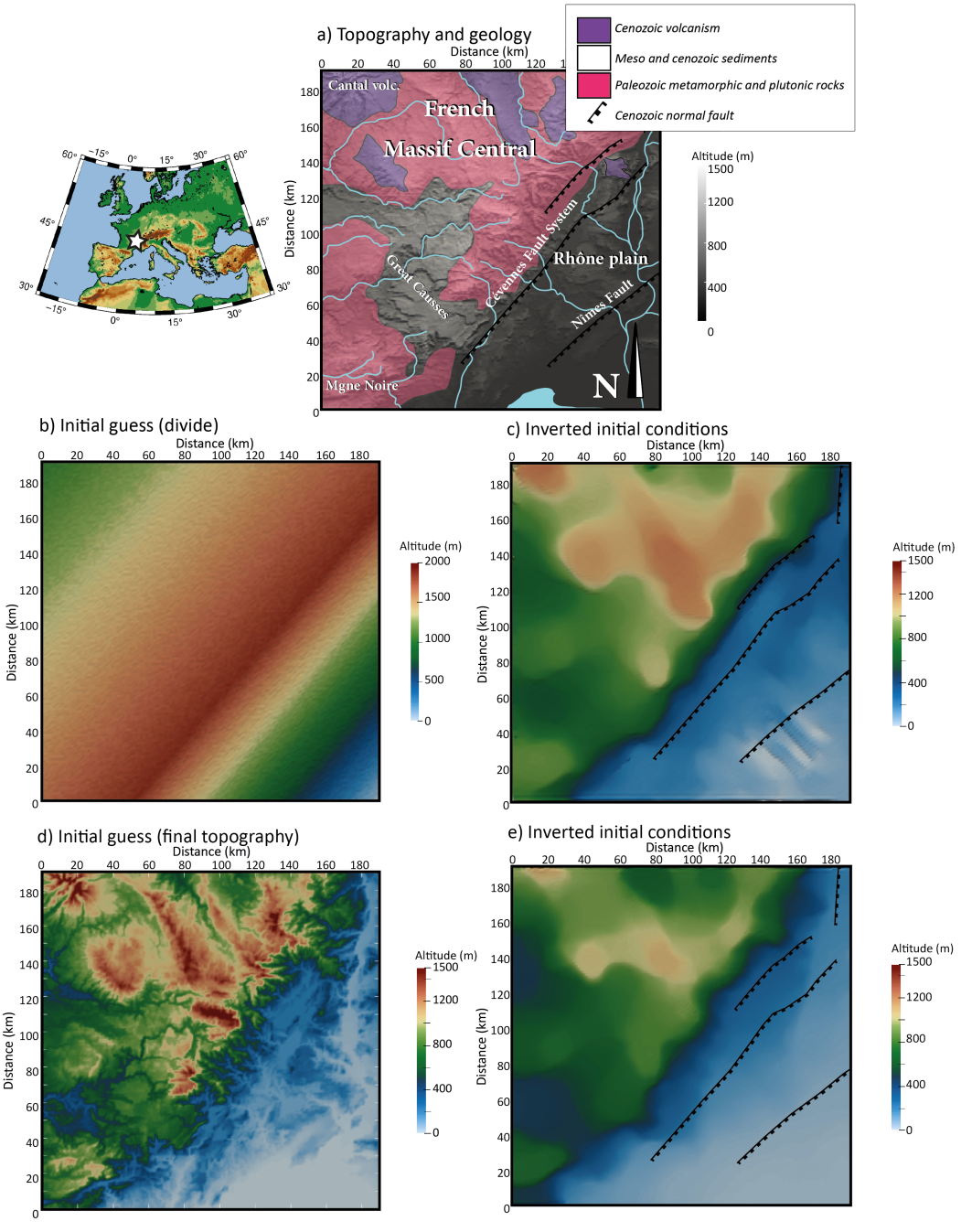

Figure 7. Inversion of initial conditions for the French Massif Central (model 7, Table 1). (a): Simplified geology (transparent colors) and present-day topography (grey shades) of the SE Massif Central (white star on left map indicates its location in western Europe) with the main cenozoic faults. (b): guess initial conditions with a NE-SW asymmetric divide; (c): inverted initial conditions with (b) as guess; (d): guess initial conditions corresponding to the current topography; (e): inverted initial conditions with (d) as guess.

https://doi.org/10.5194/egusphere-2025-1812
Preprint. Discussion started: 30 April 2025

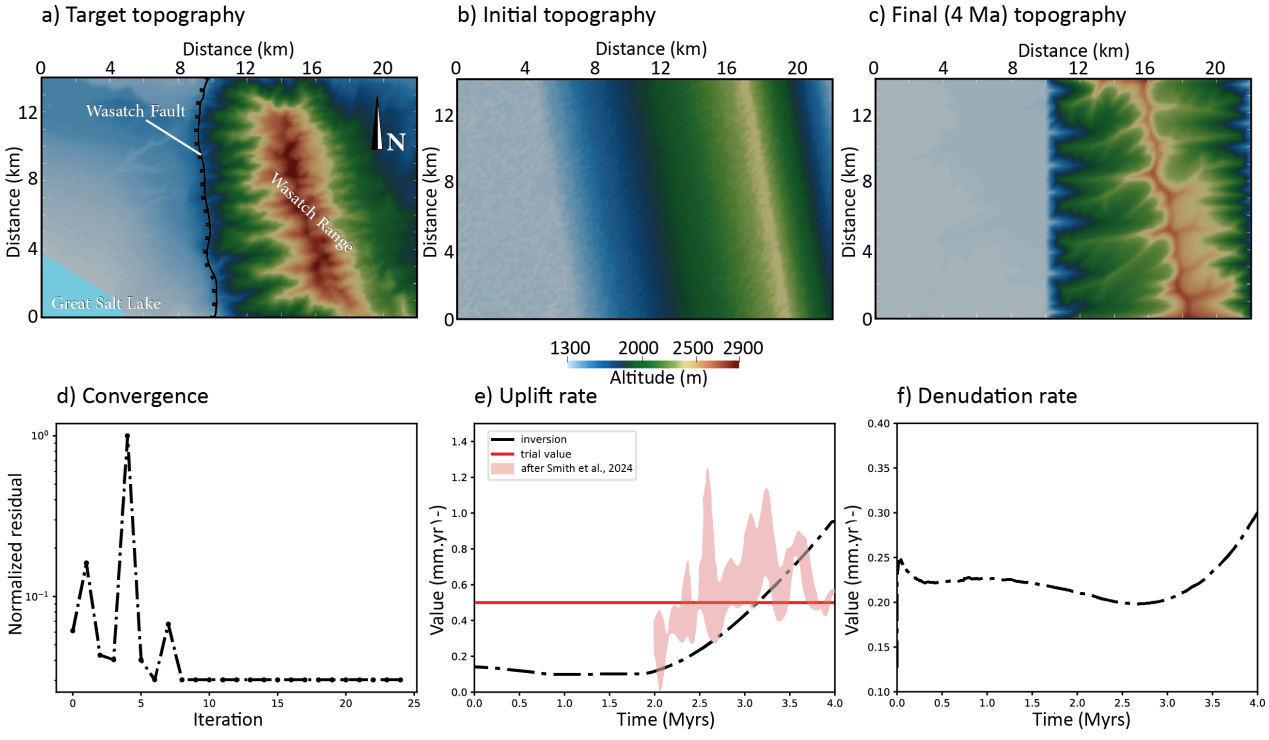

Figure 8. Inverse modelling of the Wasatch Range uplift rate (model 8, Table 1). (a): Topography of the Weber segment of the Wasatch fault used as the control parameter (white star on inset indicates its location in North America); (b): Initial topography conditions for the inverse model; (c): Modelled topography with uplift rates obtained by the inverse model; (d): model residuals; (e): Comparison between inverted uplift rates (this study) and those obtained from river longitudinal profile analysis (Smith et al., 2024), red enveloppe corresponding to 7 profiles; (f): modelled denudation rate.

observations into the inversion and to invert for a large number of parameters like the initial topography, or spatial variations κ or K_f.

For comparison, Yuan et al. (2019) conducted 100,000 forward model runs to constrain four spatially constant erosion parameters two of which define the minimum and maximum bounds of a temporally evolving fluvial incision parameter K_f (which varies linearly over time). Pedersen et al. (2018) performed approximately 13,000 forward model runs to constrain between 2 and 5 free parameters related to uplift rate variations and erosion coefficient, the uplift parameters being defined within a prescribed spatial uplift zone and allowed to vary only across discrete time intervals. While such methods can identify the best-fit model at a reasonable computational cost, they lack the capacity to precisely quantify spatial sensitivity, that is, they cannot determine which specific topographic features most strongly influence the fit to observations.

Unlike gradient-free methods, the adjoint approach can efficiently handle high-dimensional problems that would otherwise be computationally impossible. Additionally, while incorporating more complex processes (e.g., sedimentation, isostatic re-

https://doi.org/10.5194/egusphere-2025-1812
Preprint. Discussion started: 30 April 2025

bound) significantly increases computational costs for gradient-free methods, the adjoint method remains computationally feasible as the forward model is only run once.

While solving erosion as a PDE with the adjoint method offers significant advantages — such as efficient gradient computation and sensitivity analysis — it has several limitations. First, when advection velocities become high, the drainage network can become numerically unstable, leading to hazardous propagation of local extrema. This issue stems from solving the stream power law as an advection equation rather than being specific to the adjoint method itself. A second constraint lies in the need for accurate, independent computation of drainage areas. The method requires that drainage directions align as closely as possible with the true topographic gradient, since upstream information propagation along channel networks depends on this alignment.

Currently, the approach remains restricted to detachment-limited erosion scenarios where the SPL applies and where the slope exponent $n = 1$. Significant development work would be needed to extend this framework to more complex situations, such as transport-limited systems involving sediment deposition or flexural isostatic adjustment. Furthermore, incorporating additional constraints like cosmogenic exposure ages would enhance the method's applicability but remains to be implemented.

In this study, we have limited the model to simple inversions under two main assumptions: 1) except in some test cases, only one parameter is unknown, the other ones being perfectly determined; and 2) while the model can handle spatially variable erosion coefficients and initial topography, it cannot determine both temporal and spatial uplift rate variations. While such conditions are not always realistic in natural settings, this limitation is not unique to inverse problems; forward models of landscape evolution also face similar constraints. Like in forward models, another major tradeoff could arise from the underdetermination of both the initial conditions and the uplift rate, or erosion coefficients and uplift rate in the case of an actively uplifting landscape, especially if the steady-state is not yet reached. For these reasons, joint inversion of multiple parameters such as the diffusion and erodibility coefficients, as well as source and initial conditions, could improve the procedure. The challenge, however, consists in incorporating sufficient data so that the joint inversion problem is not overly under-constrained. The advantage of the adjoint approach is that it enables us to quantify the influence of each parameter on the model outcome.

Applying this method to natural cases demonstrates its potential to infer pre-incision topography or temporal variations in uplift rates, provided reasonable assumptions are made about the remaining parameters. In the case of the French Massif Central, while the age of the pre-incision topography remains uncertain, the recovered initial topography effectively highlights well-defined normal fault escarpments. This inversion proves relatively straightforward because the original fault escarpment has not been extensively degraded. Moreover, model sensibility estimates highlight a domain with a large sensitivity both to diffusion and erodibility coefficients. This domain, located along the escarpment of the Mesozoic Cevennes fault system is presently characterized by intense seasonal rains called "Cevenol episodes" due to the conjonction of a topographic barrier to southerly winds carrying the humid and warm air of the mediterranean Sea (e.g., Delrieu et al., 2005). Assuming that the erodibility coefficient K_f is directly related to the precipitation rate, we can deduce from the sensitivity maps that the Cévennes landscape evolution is very sensitive to these extreme episodes. Finally, the inversion of temporal variations in uplift rates along a segment of the Wasatch Fault is feasible due to the strong dependency of the topography — particularly river longitudinal profiles — on the uplift rate. However, as regressive erosion progressively removes evidence of the earliest landscape history, it

https://doi.org/10.5194/egusphere-2025-1812
Preprint. Discussion started: 30 April 2025

is virtually impossible to reconstruct the oldest phases of uplift. The observed discrepancies between uplift rates derived from river profile inversion and our adjoint-based approach likely stem from several key factors. First, river profile methods rely on a steady-state assumption linking channel morphology to uplift history (Goren, 2016) — an approximation that may not always be valid. Second, such approaches inherently focus on channel dynamics while neglecting hillslope processes and the rest of the landscape. Third, they typically assume temporally invariant drainage areas, ignoring catchment reorganization with time. In contrast, our adjoint method uses a reduced functional that minimizes the residual between modeled and observed topography, ensuring consistency with the range-scale morphological evolution. While this approach better captures the average landscape response, it naturally smooths short-wavelength features like knickpoints that record abrupt uplift changes.

6 Conclusion

A finite-element model that combines the Stream Power Law of fluvial incision with linear hillslope diffusion into a classic diffusion-advection equation offers several advantages. First, it enables a consistent treatment of the "slope" responsible for both the downslope movement of the surficial altered layer (simulating hillslope diffusion) and water flow along channels (fluvial incision). In this approach, both processes rely on the same topographic gradient, providing a more physically realistic framework. This contrasts to models that use a local channel slope derived from preferred drainage directions. Second, it enables the solution of the adjoint problem to invert unknown parameter values and assess the model sensitivity to these parameters, which is difficult to do with only forward models and gradient-free procedures.

Our results demonstrate that it is possible to invert spatial variations of the diffusion and erodibility coefficients, and to evaluate the landscape sensitivity to these parameters. Additionally, simple uplift scenarios involving constant or smoothly varying rock uplift rates can be effectively determined. When addressing the initial conditions of a degrading escarpment, some regularization parameters are required, yet this approach still yields consistent results with respect to the forward model.

Applications to real-world data, such as the pre-incision topography of the SE French Massif Central and the uplift rate of the Wasatch Fault in Utah, suggest that this methodology holds potential for natural case studies. In particular, we show that the dissected, linear escarpment bounding the SE part of the French Massif Central is more sensitive to hillslope diffusion and river incision than the rest of the domain. In the same region, our results suggest that, prior to intense incision by SE flowing rivers, the topography was delineated by a linear NE-SW escarpment that coincides with the trace of a major Mesozoic fault. Concerning the Wasatch fault, slip rate inversion depicts a first period of low slip rate, that has increased dramatically 2 Myrs ago.

7 Acknowledgements

Many thanks to Guillaume Duclaux for very enthousiastic and fruitful discussions on this paper.

https://doi.org/10.5194/egusphere-2025-1812
Preprint. Discussion started: 30 April 2025

8 Code availability

The code, parameter and data files are available on bitbucket (git@bitbucket.org:jourdon_anthony/laser.git).

9 Competing interests

The authors declare no competing interests.

10 Authors contribution

CP developed the code, analyzed the results and wrote the manuscript. AJ developed the code, discussed the results and participated in writing the manuscript. NC discussed the results and participated in writing the manuscript.

https://doi.org/10.5194/egusphere-2025-1812
Preprint. Discussion started: 30 April 2025

References

Armstrong, P. A., Ehlers, T. A., Chapman, D. S., Farley, K. A., and Kamp, P. J. J.: Exhumation of the central Wasatch Mountains, Utah: 1. Patterns and timing of exhumation deduced from low-temperature thermochronology data, Journal of Geophysical Research: Solid Earth, 108, https://doi.org/https://doi.org/10.1029/2001JB001708, 2003.

Barcelos, C.: Edge-preserving regularization in image restoration, Boletim (SBMAC), 7, 31–43, 2002.

Barnhart, K. R., Hutton, E. W., Tucker, G. E., Gasparini, N. M., Istanbulluoglu, E., Hobley, D. E., Lyons, N. J., Mouchene, M., Nudurupati, S. S., Adams, J. M., et al.: Landlab v2. 0: a software package for Earth surface dynamics, Earth Surface Dynamics, 8, 379–397, https://doi.org/10.5194/esurf-8-379-2020, 2020a.

Barnhart, K. R., Tucker, G. E., Doty, S. G., Shobe, C. M., Glade, R. C., Rossi, M. W., and Hill, M. C.: Inverting Topography for Landscape Evolution Model Process Representation: 1. Conceptualization and Sensitivity Analysis, Journal of Geophysical Research: Earth Surface, 125, e2018JF004 961, https://doi.org/https://doi.org/10.1029/2018JF004961, 2020b.

Barnhart, K. R., Tucker, G. E., Doty, S. G., Shobe, C. M., Glade, R. C., Rossi, M. W., and Hill, M. C.: Inverting Topography for Landscape Evolution Model Process Representation: 2. Calibration and Validation, Journal of Geophysical Research: Earth Surface, 125, e2018JF004 963, https://doi.org/https://doi.org/10.1029/2018JF004963, 2020c.

Braun, J.: Pecube: a new finite-element code to solve the 3D heat transport equation including the effects of a time-varying, finite amplitude surface topography, Computers and Geosciences, 29, 787–794, https://doi.org/https://doi.org/10.1016/S0098-3004(03)00052-9, 2003.

Braun, J. and Willett, S. D.: A very efficient O(n), implicit and parallel method to solve the stream power equation governing fluvial incision and landscape evolution, Geomorphology, 180-181, 170–179, https://doi.org/https://doi.org/10.1016/j.geomorph.2012.10.008, 2013.

Braun, J., van der Beek, P., Valla, P., Robert, X., Herman, F., Glotzbach, C., Pedersen, V., Perry, C., Simon-Labric, T., and Prigent, C.: Quantifying rates of landscape evolution and tectonic processes by thermochronology and numerical modeling of crustal heat transport using PECUBE, Tectonophysics, 524-525, 1–28, https://doi.org/https://doi.org/10.1016/j.tecto.2011.12.035, 2012.

Carretier, S., Martinod, P., Reich, M., and Godderis, Y.: Modelling sediment clasts transport during landscape evolution, Earth Surface Dynamics, 4, 237–251, https://doi.org/10.5194/esurf-4-237-2016, 2016.

Celia, M. A., Russell, T. F., Herrera, I., and Ewing, R. E.: An Eulerian-Lagrangian localized adjoint method for the advection-diffusion equation, Advances in Water Resources, 13, 187–206, https://doi.org/https://doi.org/10.1016/0309-1708(90)90041-2, 1990.

Chandra, R., Azam, D., Müller, R. D., Salles, T., and Cripps, S.: Bayeslands: A Bayesian inference approach for parameter uncertainty quantification in Badlands, Computers and Geosciences, 131, 89–101, https://doi.org/https://doi.org/10.1016/j.cageo.2019.06.012, 2019.

Clare, M. C., Kramer, S. C., Cotter, C. J., and Piggott, M. D.: Calibration, inversion and sensitivity analysis for hydro-morphodynamic models through the application of adjoint methods, Computers and Geosciences, 163, 105 104, https://doi.org/https://doi.org/10.1016/j.cageo.2022.105104, 2022.

Croissant, T. and Braun, J.: Constraining the stream power law: a novel approach combining a landscape evolution model and an inversion method, Earth Surface Dynamics, 2, 155–166, https://doi.org/10.5194/esurf-2-155-2014, 2014.

Davy, P. and Lague, D.: Fluvial erosion/transport equation of landscape evolution models revisited, Journal of Geophysical Research: Earth Surface, 114, https://doi.org/https://doi.org/10.1029/2008JF001146, 2009.

Delrieu, G., Nicol, J., Yates, E., Kirstetter, P.-E., Creutin, J.-D., Anquetin, S., Obled, C., Saulnier, G.-M., Ducrocq, V., Gaume, E., Payrastre, O., Andrieu, H., Ayral, P.-A., Bouvier, C., Neppel, L., Livet, M., Lang, M., du Châtelet, J. P., Walpersdorf, A., and Wobrock, W.: The

https://doi.org/10.5194/egusphere-2025-1812
Preprint. Discussion started: 30 April 2025

Catastrophic Flash-Flood Event of 8–9 September 2002 in the Gard Region, France: A First Case Study for the Cévennes–Vivarais Mediterranean Hydrometeorological Observatory, Journal of Hydrometeorology, 6, 34 – 52, https://doi.org/10.1175/JHM-400.1, 2005.

Ehlers, T. A., Willett, S. D., Armstrong, P. A., and Chapman, D. S.: Exhumation of the central Wasatch Mountains, Utah: 2. Thermokinematic model of exhumation, erosion, and thermochronometer interpretation, Journal of Geophysical Research: Solid Earth, 108, https://doi.org/https://doi.org/10.1029/2001JB001723, 2003.

Fauquette, S., Suc, J.-P., Popescu, S.-M., Guillocheau, F., Violette, S., Jost, A., Robin, C., Briais, J., and Baby, G.: Pliocene uplift of the Massif Central (France) constrained by the palaeoelevation quantified from the pollen record of sediments preserved along the Cantal Stratovolcano (Murat area), Journal of the Geological Society, 177, 923–938, https://doi.org/10.1144/jgs2020-010, 2020.

Friedrich, A. M., Wernicke, B. P., Niemi, N. A., Bennett, R. A., and Davis, J. L.: Comparison of geodetic and geologic data from the Wasatch region, Utah, and implications for the spectral character of Earth deformation at periods of 10 to 10 million years, Journal of Geophysical Research: Solid Earth, 108, https://doi.org/https://doi.org/10.1029/2001JB000682, 2003.

Givoli, D.: A tutorial on the adjoint method for inverse problems, Computer Methods in Applied Mechanics and Engineering, 380, 113 810, https://doi.org/https://doi.org/10.1016/j.cma.2021.113810, 2021.

Goren, L.: A theoretical model for fluvial channel response time during time-dependent climatic and tectonic forcing and its inverse applications, Geophysical Research Letters, 43, 10,753–10,763, https://doi.org/10.1002/2016GL070451, 2016.

Ham, D. A., Kelly, P. H. J., Mitchell, L., Cotter, C. J., Kirby, R. C., Sagiyama, K., Bouziani, N., Vorderwuelbecke, S., Gregory, T. J., Betteridge, J., Shapero, D. R., Nixon-Hill, R. W., Ward, C. J., Farrell, P. E., Brubeck, P. D., Marsden, I., Gibson, T. H., Homolya, M., Sun, T., McRae, A. T. T., Luporini, F., Gregory, A., Lange, M., Funke, S. W., Rathgeber, F., Bercea, G.-T., and Markall, G. R.: Firedrake User Manual, Imperial College London and University of Oxford and Baylor University and University of Washington, first edition edn., https://doi.org/10.25561/104839, 2023.

Hobley, D. E., Adams, J. M., Nudurupati, S. S., Hutton, E. W., Gasparini, N. M., Istanbulluoglu, E., and Tucker, G. E.: Creative computing with Landlab: an open-source toolkit for building, coupling, and exploring two-dimensional numerical models of Earth-surface dynamics, Earth Surface Dynamics, 5, 21–46, https://doi.org/10.5194/esurf-5-21-2017, 2017.

Hutton, E., Barnhart, K., Hobley, D., Tucker, G., Nudurupati, S., Adams, J., Gasparini, N., Shobe, C., Strauch, R., Knuth, J., Mouchene, M., Lyons, N., Litwin, D., Glade, R., Giuseppecipolla95, Manaster, A., Abby, L., Thyng, K., and Rengers, F.: Landlab, software, https://doi.org/10.5281/zenodo.595872, 2020.

NASA: Shuttle Radar Topography Mission (SRTM) Global. Distributed by OpenTopography, https://doi.org/https://doi.org/10.5069/G9445JDF, 2013.

Olivetti, V., Godard, V., and Bellier, O.: Cenozoic rejuvenation events of Massif Central topography (France): Insights from cosmogenic denudation rates and river profiles, Earth and Planetary Science Letters, 444, 179–191, https://doi.org/https://doi.org/10.1016/j.epsl.2016.03.049, 2016.

Parkinson, S., Funke, S., Hill, J., Piggott, M., and Allison, P.: Application of the adjoint approach to optimise the initial conditions of a turbidity current with the AdjointTurbidity 1.0 model, Geoscientific Model Development, 10, 1051–1068, https://doi.org/10.5194/gmd-10-1051-2017, 2017.

Pedersen, V. K., Braun, J., and Huismans, R. S.: Eocene to mid-Pliocene landscape evolution in Scandinavia inferred from offshore sediment volumes and pre-glacial topography using inverse modelling, Geomorphology, 303, 467–485, https://doi.org/https://doi.org/10.1016/j.geomorph.2017.11.025, 2018.

https://doi.org/10.5194/egusphere-2025-1812
Preprint. Discussion started: 30 April 2025

Salles, T.: Badlands : A parallel basin and landscape dynamics model, SoftwareX, 5, 195–202, https://doi.org/10.1016/j.softx.2016.08.005, 2016.

Salles, T. and Hardiman, L.: Badlands: An open-source, flexible and parallel framework to study landscape dynamics, Computers and Geosciences, 91, 77–89, https://doi.org/http://dx.doi.org/10.1016/j.cageo.2016.03.011, 2016.

Simpson, G. and Schlunegger, F.: Topographic evolution and morphology of surfaces evolving in response to coupled fluvial and hillslope sediment transport, Journal of Geophysical Research: Solid Earth, 108, https://doi.org/https://doi.org/10.1029/2002JB002162, 2003.

Smith, A. G. G., Fox, M., Moore, J. R., Miller, S. R., Goren, L., Morriss, M. C., and Carter, A.: One Million Years of Climate-Driven Rock Uplift Rate Variation on the Wasatch Fault Revealed by Fluvial Topography, American Journal of Science, 324, 1, https://doi.org/10.2475/001c.92194, 2024.

Stock, G. M., Frankel, K. L., Ehlers, T. A., Schaller, M., Briggs, S. M., and Finkel, R. C.: Spatial and temporal variations in denudation of the Wasatch Mountains, Utah, USA, Lithosphere, 1, 34–40, https://doi.org/10.1130/L15.1, 2009.

Strong, D. and Chan, T.: Edge-preserving and scale-dependent properties of total variation regularization, Inverse Problems, 19, S165, https://doi.org/10.1088/0266-5611/19/6/059, 2003.

Séranne, M., Coueffé, R., Husson, E., Baral, C., and Villard, J.: The transition from Pyrenean shortening to Gulf of Lion rifting in Languedoc (South France) – A tectonic-sedimentation analysis, Bulletin de la Société Géologique de France, 192, https://doi.org/10.1051/bsgf/2021017, 2021.

Talagrand, O.: Variational assimilation, Data assimilation: making sense of observations, pp. 41–67, 2010.

Tao, S., Li, Y., and Mugume, I.: Model terrain correction using variational adjoint method with Tikhonov-total variation regularization, Journal of Physics: Conference Series, 1176, 022 034, https://doi.org/10.1088/1742-6596/1176/2/022034, 2019.

Tarboton, D.: A new method for the determination of flow directions and upslope areas in grid digital elevation models, Water Resources Research, 33, 309–319, https://doi.org/https://doi.org/10.1029/96WR03137, 1997.

Tucker, G., Lancaster, S., Gasparini, N., and Bras, R.: The Channel-Hillslope Integrated Landscape Development Model (CHILD), pp. 349–388, Springer US, Boston, MA, https://doi.org/10.1007/978-1-4615-0575-4_12, 2001.

Tucker, G. E. and Hancock, G. R.: Modelling landscape evolution, Earth Surface Processes and Landforms, 32, 28–50, https://doi.org/10.1002/eps.1952, 2010.

Tucker, G. E. and Slingerland, R. L.: Erosional dynamics, flexural isostasy, and long-lived escarpments: A numerical modeling study, Journal of Geophysical Research: Solid Earth, 99, 12 229–12 243, https://doi.org/https://doi.org/10.1029/94JB00320, 1994.

Whipple, K. and Tucker, G.: Dynamics of the stream-power river incision model: Implications for height limits of mountain ranges, landscape response timescales, and research needs, Journal of Geophysical Research, 104, 17,661–17,674, 1999.

Yuan, X., Braun, J., Guerit, L., Simon, B., Bovy, B., Rouby, D., Robin, C., and Jiao, R.: Linking continental erosion to marine sediment transport and deposition: A new implicit and O(n) method for inverse analysis, Earth and Planetary Science Letters, 524, 115 728, https://doi.org/https://doi.org/10.1016/j.epsl.2019.115728, 2019.